ARTICLES
PUBLISHED ONLINE: 21 JULY 2013 | DOI: 10.1038/NPHOTON.2013.181
nature photonics

Versatile surface plasmon resonance of carbon-dot-supported silver nanoparticles in polymer optoelectronic devices

Hyosung Choi[1], Seo-Jin Ko[1], Yuri Choi[1], Piljae Joo[1], Taehyo Kim[1], Bo Ram Lee[2], Jae-Woo Jung[3], Hee Joo Choi[4], Myoungsik Cha[4], Jong-Ryul Jeong[3], In-Wook Hwang[5], Myoung Hoon Song[2], Byeong-Su Kim[1]* and Jin Young Kim[1]*

The coupling of surface plasmons and excitons in organic materials can improve the performance of organic optoelectronic devices. Here, we prepare carbon-dot-supported silver nanoparticles (CD–Ag nanoparticles) using the carbon dots both as a reducing agent and a template to fabricate solution-processable polymer light-emitting diodes and polymer solar cells. The surface plasmon resonance effect of CD–Ag nanoparticles allows significant radiative emission and additional light absorption, leading to remarkably enhanced current efficiency of 27.16 cd A^{-1} and a luminous efficiency of 18.54 lm W^{-1} in polymer light-emitting diodes as well as a power conversion efficiency of 8.31% and an internal quantum efficiency of 99% in polymer solar cells compared with control devices (current efficiency = 11.65 cd A^{-1} and luminous efficiency = 6.33 lm W^{-1} in polymer light-emitting diodes; power conversion efficiency = 7.53% and internal quantum efficiency = 91% in polymer solar cells). These results demonstrate that CD–Ag nanoparticles constitute a versatile and effective route for achieving high-performance polymer optoelectronic devices.

Most semiconducting optoelectronic devices (OEDs) are currently based on inorganic materials such as GaN (for light-emitting diodes, LEDs) and silicon (for solar cells). However, the cost of device fabrication using these materials is increasing because of their limited reserves and the necessarily complex processing. There is therefore significant interest in developing thin-film OEDs made from other semiconductors, including ZnSe, $CuInSe_2$, CdTe and organic semiconductors[1–5]. Among these materials, organic semiconductors have received a great deal of attention for use in next-generation OEDs because of the potential for low-cost and large-area fabrication using solution processing. Although extensive efforts to develop new materials and device architectures have enhanced the performance of these devices[4,6–9], further improvements in device efficiency are still necessary if there is to be widespread use and commercialization of these technologies.

Surface plasmons are collective oscillations of free electrons in a metal at an interface with a dielectric[10,11]. Excitation of surface plasmons by light at the incident wavelength at which resonance occurs can result in strong light scattering, with the appearance of intense surface plasmon absorption bands and an enhancement of the local electromagnetic fields[12,13]. The coupling effect between excitons and surface plasmons, which is caused by the overlap of the local electromagnetic field of excitons in the emissive layer and surface plasmons, leads to significant radiative emission through effective energy transfer in polymer LEDs (PLEDs)[11,14,15]. In addition, metal nanoparticles can act as effective antennas for incident light, enabling the storage of the incident energy in localized surface plasmon modes and leading to the photogeneration of excitons in polymer solar cells (PSCs)[13]. Plasmonic PLEDs therefore require an enhanced radiative rate without a substantial increase in light absorption, whereas plasmonic PSCs need to maximize light absorption while minimizing radiative decay or non-radiative losses[16]. Thus, despite their strong potential for improving device efficiency, there are few reports on metal nanoparticles simultaneously enhancing performance in both PLED and PSC devices[17].

As an alternative to traditional semiconducting quantum dot nanoparticles, carbogenic nanoparticles (also known as carbon dots) have recently received significant attention because of their interesting physical, optical and chemical properties, including photoluminescence, photostability and electron transfer behaviour[18]. Following the early report by Sun and co-workers in 2006[19], significant research efforts have been expended to produce carbon dots with controlled dimensions and surface properties, using many techniques, including combustion, laser ablation, microwave processing, silica template methods and deoxygenation of natural carbon sources[20–24]. Photoinduced electron transfer can be enhanced by the surface passivation of carbon dots, which affords new opportunities to use them for light energy conversion and related applications[25,26].

Here, we demonstrate highly efficient PLEDs and PSCs using surface plasmon resonance (SPR) enhancement with carbon-dot-supported silver nanoparticles (CD–Ag nanoparticles). The CD–Ag nanoparticles have several advantages over conventional metal nanoparticles. First, the excellent electron-donating capability of photoexcited carbon dots enables fast reduction of metal salts to corresponding metal nanoparticles on the surfaces of the carbon

[1]Interdisciplinary School of Green Energy and KIER-UNIST Advanced Center for Energy, Ulsan National Institute of Science and Technology (UNIST), Ulsan 689-798, Korea, [2]School of Mechanical and Advanced Materials Engineering and KIST-UNIST Ulsan Center for Convergent Materials, Ulsan National Institute of Science and Technology (UNIST), Banyeon-ri 100, Ulsan 689-798, Korea, [3]Department of Materials Science and Engineering and Graduate School of Green Energy Technology, Chungnam National University, Daejeon 305-764, Korea, [4]Department of Physics, Pusan National University, Busan 609-735, Korea, [5]Advanced Photonics Research Institute, Gwangju Institute of Science and Technology, Gwangju 500-712, Korea.
*e-mail: bskim19@unist.ac.kr; jykim@unist.ac.kr

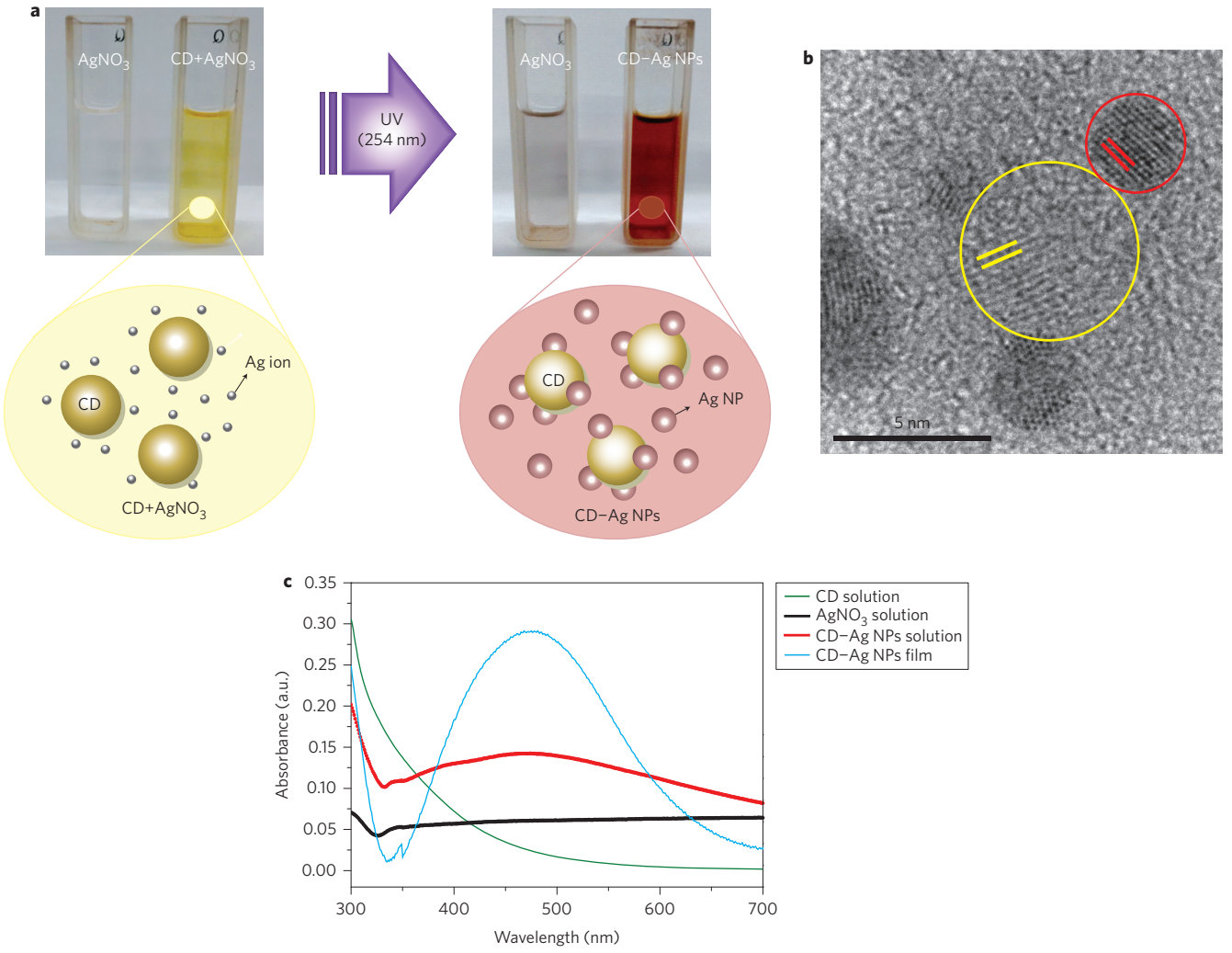

Figure 1 | Schematic illustration and characterization of CD-Ag nanoparticles. a, Photographs and schematic illustration of $AgNO_3$ and carbon dot (CD) + $AgNO_3$ blend solutions before (left) and after (right) ultraviolet irradiation. **b**, HR-TEM image of CD–Ag nanoparticles (NPs). Yellow and red circles indicate the presence of carbon dots and silver nanoparticles, respectively. The two parallel lines in yellow and red show the distinguishable lattice fringes (3.2 Å and 2.1 Å) of carbon dots and silver nanoparticles, respectively. Scale bar, 5 nm. **c**, Comparison of UV–vis absorption spectra of CD–Ag nanoparticles in solution and in a film, and carbon dot and $AgNO_3$ solutions after ultraviolet irradiation.

dots[25]. During this process, the carbon dot also acts as a template, leading to a metal-nanoparticle-decorated surface of the dot. Second, the synthesis of the CD–Ag nanoparticles is simple and requires only basic equipment (20 min exposure to a ultraviolet lamp). Third, because of their low-temperature solution processability, CD–Ag nanoparticles are compatible with large-area, roll-to-roll mass production techniques and are suitable for printed electronic devices. Fourth, the clustering effect of silver nanoparticles on the carbon dots results in broad light absorption from electric field enhancement at the gap between the silver nanoparticles, without any changes in the size or shape of the nanoparticles. This templating and clustering effect of the carbon dot supports has a dramatic effect on the plasmonic properties and absorption of the nanoparticles, and represents a critical advance over unsupported nanoparticles, allowing record efficiencies to be achieved in both PLED and PSC devices.

From the many available synthetic methods[19,20,22,23,27–30], we chose to prepare the carbon dots using thermal decomposition of the oligosaccharide alpha-cyclodextrin, followed by surface passivation with poly(ethylene glycol) (PEG). The carbon dots were photoexcited with ultraviolet irradiation in the presence of $AgNO_3$, which reduced the Ag^+ ions to silver nanoparticles via electron transfer from the photoexcited carbon dots[31]. In this procedure, the silver nanoparticles tend to form on the surface of the carbon dots (Fig. 1a). After ultraviolet irradiation, the $AgNO_3$/carbon dot solution changes from yellow to dark brown, indicating the conversion of Ag^+ ions to silver nanoparticles (Fig. 1a, Supplementary Fig. S1). Details of the CD–Ag nanoparticle synthesis are provided in the Methods. A high-resolution transmission electron microscopy (HR-TEM) image of the CD–Ag nanoparticles is presented in Fig. 1b. The CD–Ag nanoparticles have average diameters and distinguishing lattice fringes of ~6 nm and 3.2 Å for the carbon dots and ~3 nm and 2.1 Å for the silver nanoparticles, respectively. UV–vis absorption spectra of CD–Ag nanoparticles in solution and as thin films, in addition to $AgNO_3$ and carbon dot solutions, are presented in Fig. 1c. After ultraviolet irradiation for 20 min, surface plasmon peaks of the silver nanoparticles appear at ~460 nm, both in solution and in the film, but no specific peak for silver nanoparticles is observed in the control set of ultraviolet-irradiated $AgNO_3$ or carbon dot solutions. In contrast to the SPR peaks obtained for free silver nanoparticles with a similar size (420 nm)[32], CD–Ag nanoparticles show redshifted SPR peaks at 460 nm (Supplementary Fig. S2).

To explore the shift of the SPR peak and the electric field enhancement caused by the CD–Ag nanoparticles, we simulated the

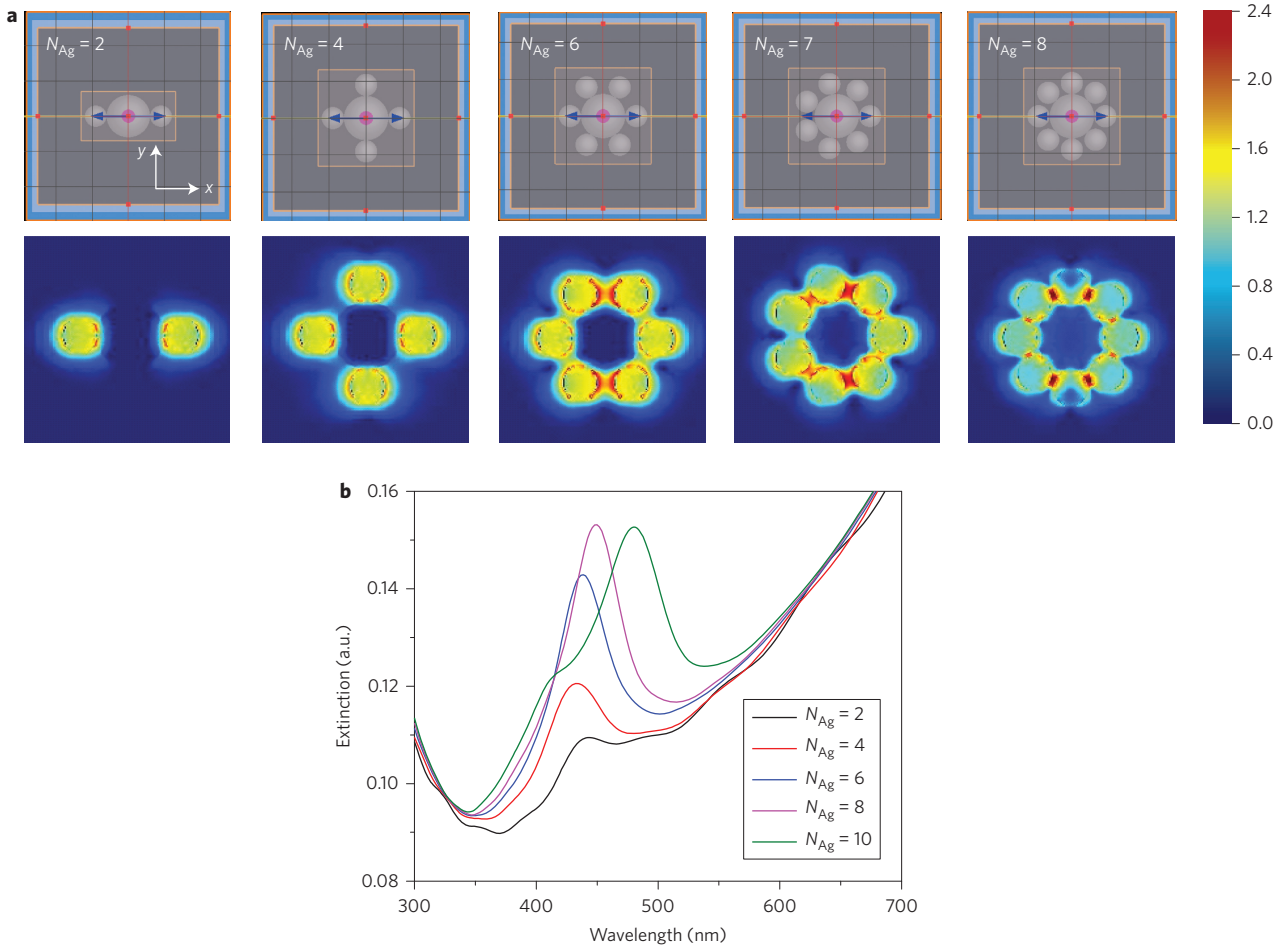

Figure 2 | Simulation of the electromagnetic field distribution for CD–Ag nanoparticles. a,**b**, Simulated electric field distribution (**a**) and extinction spectrum (**b**) for CD–Ag nanoparticles as a function of the number of silver nanoparticles on the surface of the carbon dots (N_{Ag}). The magnitude of the enhanced electric field intensity is indicated by the colour scale.

electric field distribution using the three-dimensional finite-difference time-domain (FDTD) method. Figure 2a presents the simulated electric field intensity distribution and predicted extinction spectra of CD–Ag nanoparticles as a function of the number of silver nanoparticles formed on the surface of the carbon dots. According to the TEM results, there are many possibilities regarding the number of silver nanoparticles that can form on the surface of each carbon dot; accordingly, we performed a simulation for varying numbers of silver nanoparticles (from 2 to 8). We observed that increasing the number of silver nanoparticles on the carbon dot surface makes the electronic coupling between CD–Ag and Ag–Ag stronger, leading to an electric field enhancement at the gap between the silver nanoparticles (Fig. 2a) and broadly redshifted extinction spectra (Fig. 2b). In contrast, the control simulation for free silver nanoparticles without the carbon dots showed the highest electric field intensity in the vicinity of the substrate, with a sharp extinction spectrum at 425 nm (Supplementary Fig. S3). These simulation results are consistent with experimental UV–vis absorption spectra of free silver nanoparticles and CD–Ag nanoparticles (Supplementary Figs S2, S3). The broad UV–vis absorption spectrum of CD–Ag nanoparticles with an SPR peak at 460 nm is attributed to the ensemble light absorption resulting from the clustering effect of the silver nanoparticles on the carbon dot. Furthermore, it should be highlighted that the CD–Ag nanoparticles can tune the SPR absorption band without any changes to the size and shape of the silver nanoparticles, while maximizing the SPR effect for optoelectronic applications.

To confirm the successful formation of CD–Ag nanoparticles, we performed high-resolution X-ray photoelectron spectroscopy (XPS) and Raman spectroscopy. The XPS results provided evidence of nanoparticle formation and changes in the surface functional groups of the carbon dots (Supplementary Fig. S4, Table S1). Raman spectroscopy also showed an enhanced Raman signal for the PEG groups on the carbon dot surface from the formation of metal nanoparticles (Supplementary Fig. S5). Furthermore, to elucidate the effect of CD–Ag nanoparticles on the fluorescence of the emissive polymer layer, we performed various measurements, including steady-state photoluminescence, photoluminescence quantum efficiency (PLQE), confocal laser scanning microscopy (CLSM), time-correlated single photon counting (TCSPC) and amplified spontaneous emission (ASE) behaviour.

Figure 3a presents the steady-state photoluminescence spectra for Super Yellow (SY), poly(3,4-ethylenedioxythiophene):polystyrene sulphonic acid (PEDOT:PSS/SY) and CD–Ag nanoparticles/PEDOT:PSS/SY films coated on glass substrates. As a control, we prepared SY films without the CD–Ag nanoparticles. Negligible changes in the thickness and morphology of the SY film result from the CD–Ag nanoparticles (Supplementary Table S2). Among the spectra, the PEDOT:PSS/SY film showed the lowest photoluminescence value because of significant exciton quenching at the PEDOT:PSS/SY interface[33], whereas the intensity of the CD–Ag nanoparticles/PEDOT:PSS/SY film was ~30% higher than the film without CD–Ag nanoparticles. The PLQE measurement resulted in values of 14.6% for SY, 12.5% for PEDOT:PSS/SY and 14.9% for CD–Ag

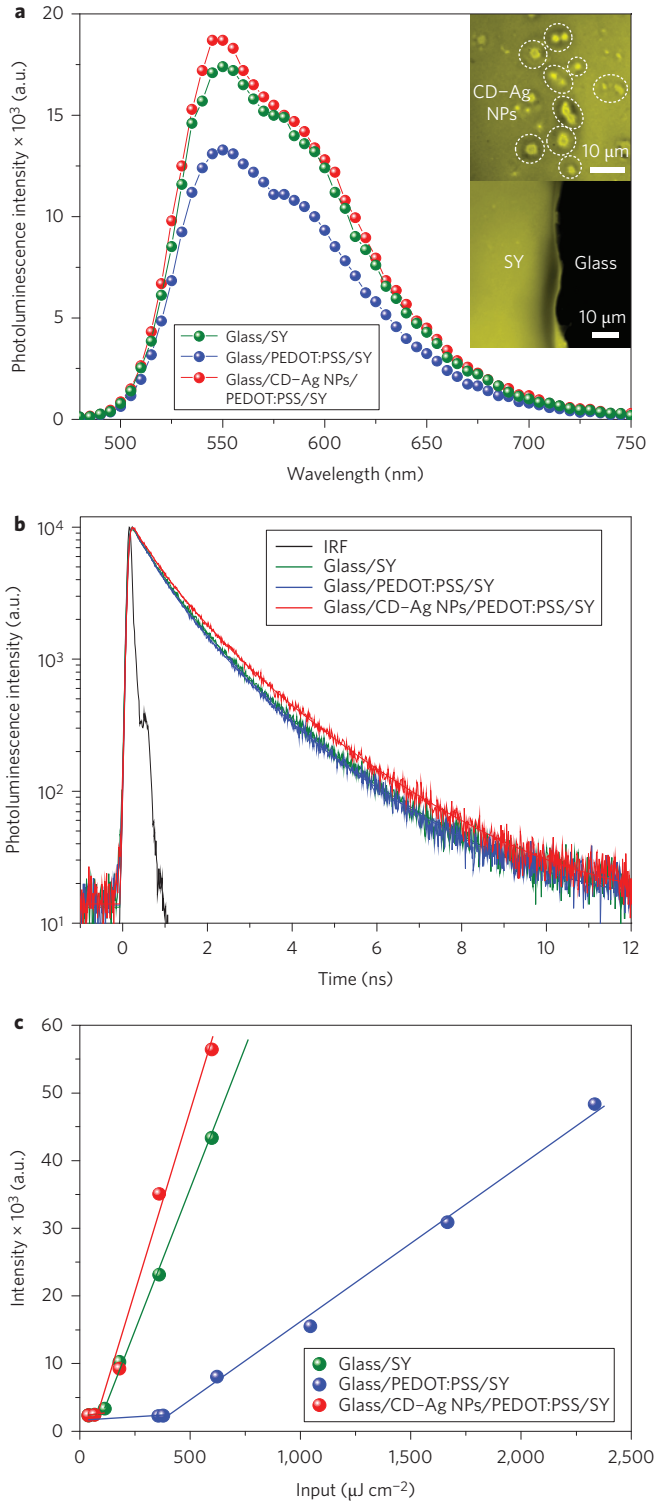

Figure 3 | Effect of CD–Ag nanoparticles on the fluorescence of polymer films. a–c, Steady-state photoluminescence spectra (**a**), photoluminescence decay profile (**b**) and ASE threshold behaviour (**c**) of the SY film. For comparison, PEDOT:PSS/SY films with and without CD–Ag nanoparticles (NPs) on glass substrates were included. Inset (**a**): confocal scanning microscope images of the SY film without (bottom) and with (top) CD–Ag nanoparticles. Scale bars, 10 μm. IRF, instrument response function.

nanoparticles/PEDOT:PSS/SY films (Supplementary Table S3). These results are in good agreement with steady-state photoluminescence data. The CLSM results also support the fluorescence emission enhancement by CD–Ag nanoparticles. The fluorescence of SY thin films with CD–Ag nanoparticles is thought to be a combination of fluorescence produced by direct excitation with the weak laser field and enhanced fluorescence produced by SY within the near-field of the CD–Ag nanoparticles. Because the confocal images show the relative fluorescence intensity, we segregated the regions of SY (yellow area) and bare glass (black area) (bottom image in Fig. 3a inset). In the SY films with CD–Ag nanoparticles, we observed bright spots (dotted lines in the top image in Fig. 3a inset), which correspond to clusters of CD–Ag nanoparticles. The fluorescence intensity of the bright spots is a factor of two to three higher than the SY background region at an excitation wavelength of 473 nm.

The photoluminescence decay profiles observed for SY, PEDOT/SY and CD–Ag nanoparticles/PEDOT:PSS/SY films are presented in Fig. 3b. From the decay values, the average photoluminescence decay time (exciton lifetime) is calculated to be 0.747 ns for SY, 0.704 ns for PEDOT:PSS/SY and 0.825 ns for CD–Ag nanoparticles/PEDOT:PSS/SY (Supplementary Table S4). The exciton lifetime of SY is decreased by exciton quenching of PEDOT:PSS, whereas the lifetime is increased in the CD–Ag nanoparticles/PEDOT:PSS/SY film in concert with the increased photoluminescence intensity (shown in Fig. 3a).

To confirm the SPR effect of CD–Ag nanoparticles on the fluorescence of the emissive polymer layer, the ASE behaviour was observed in different configurations (Fig. 3c). Samples were excited with a stripe-shaped pump beam (0.009 cm^2), and the emission spectra were measured from the substrate edges. Among the films, the CD–Ag nanoparticles/PEDOT:PSS/SY film showed the lowest threshold value of 80.8 μJ cm^{-2} (compared with 104.3 μJ cm^{-2} for SY and 402.7 μJ cm^{-2} for the PEDOT:PSS/SY film; Supplementary Fig. S6) and the highest ASE efficiency (slope), because of the enhanced optical gain caused by the SPR effect of the CD–Ag nanoparticles (Fig. 3c). The ASE is fundamentally related to exciton lifetime. Specifically, a long exciton lifetime is one of the prerequisites for ASE behaviour[34,35]. Compared to the structure without CD–Ag nanoparticles, ASE occurs more readily because of the enhanced exciton lifetimes caused by the SPR effect of CD–Ag nanoparticles. In light-emitting field-effect transistors based on fluorescent polymers, distributed feedback structures have shown estimated threshold current densities of ~60 kA cm^{-2} for lasing[36]. Thus, electrically driven laser devices might be realized with a combination of the SPR effect using metal nanoparticles and a distributed feedback structure.

We investigated the use of CD–Ag nanoparticles as plasmonic materials in PLEDs and PSCs. First, we fabricated fluorescent PLEDs to investigate the ability of CD–Ag nanoparticles to enhance the light-emitting properties of PLEDs. The device structure used was glass/indium tin oxide (ITO)/CD–Ag nanoparticles/PEDOT:PSS/SY/LiF/Al (Fig. 4a). Other than the LiF and aluminium cathode, which was deposited by vacuum thermal evaporation, all other layers were sequentially deposited onto ITO using spin coating. Although LEDs based on phosphorescent materials exhibit high electroluminescent efficiency, a more complex radiative process is involved and includes singlet–triplet energy transfer. We therefore used a fluorescent emitting polymer to focus on the effect of CD–Ag nanoparticles on singlet exciton emission. The PLED characteristics of devices with and without CD–Ag nanoparticles are plotted in Fig. 4b–d, and the results are summarized in Table 1. The device with CD–Ag nanoparticles showed a similar current density and reduced voltage for maximum luminance compared with the device without CD–Ag nanoparticles; however, the maximum luminance values are almost the same in both devices (46,460 cd m^{-2} at 9.8 V for devices with CD–Ag nanoparticles and 46,320 cd m^{-2} at 11.6 V for control devices), as shown Fig. 4b. The current efficiency and

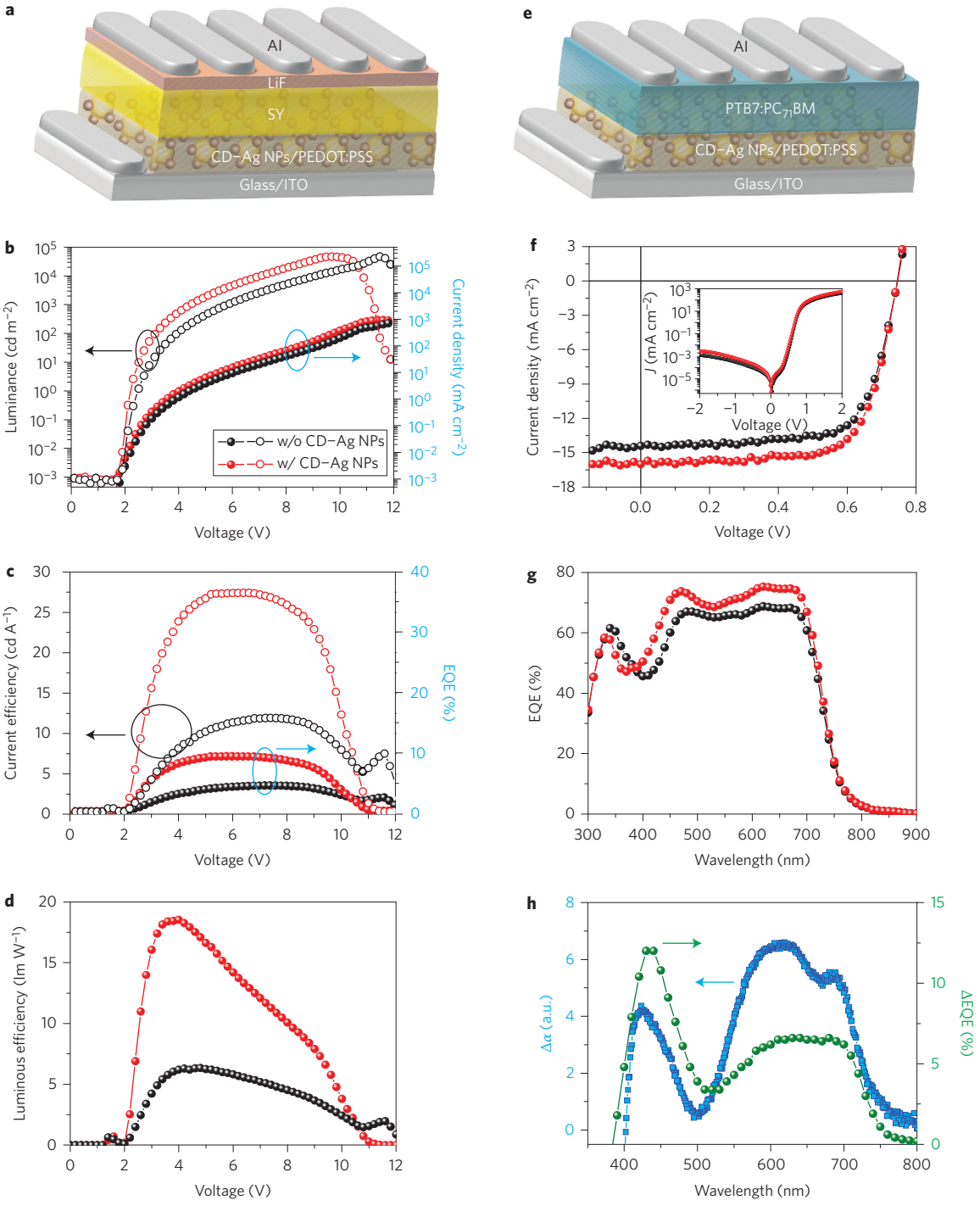

Figure 4 | Device structure and characteristics of polymer OEDs incorporating CD–Ag nanoparticles. a–d, Device structure (**a**), luminance and current density (**b**), current efficiency and EQE (**c**) and luminous efficiency (**d**) of PLEDs with and without CD–Ag nanoparticles (NPs). **e–g**, Device structure (**e**), *J–V* characteristics under AM1.5 illumination (at 100 mW cm^{-2}) (**f**) and EQE (**g**) of PSCs with and without CD–Ag nanoparticles. Inset (**f**): *J–V* characteristics under dark conditions plotted on a semilogarithmic scale. **h**, Comparison of enhanced EQE with absorption changes caused by CD–Ag nanoparticles.

external quantum efficiency (EQE) were 27.16 cd A^{-1} and 9.07%, respectively, for the device with CD–Ag nanoparticles (Fig. 4c). These values are more than twice as large as those for the device without CD–Ag nanoparticles (current efficiency = 11.65 cd A^{-1}, EQE = 4.26%). In particular, the device with CD–Ag nanoparticles showed an extremely high luminous efficiency of 18.54 lm W^{-1} (Fig. 4d). This luminous efficiency value is approximately three times higher than that of the device without CD–Ag nanoparticles (luminous efficiency = 6.33 lm W^{-1}). These current and luminous efficiencies are the highest values reported to date in plasmonic PLEDs (Supplementary Table S5).

We extended the use of CD–Ag nanoparticles to PSCs based on a mixture of poly[[4,8-bis[(2-ethylhexyl)oxy]benzo[1,2-b:4,5-b']-dithiophene-2,6-diyl][3-fluoro-2-[(2-ethylhexyl)carbonyl]thieno-[3,4-b]thiophenediyl]] (PTB7) and [6,6]-phenyl-C_{71} butyric acid methyl ester ($PC_{71}BM$) (PTB7:$PC_{71}BM$) as an active layer. The device structure employed was a glass/ITO/CD–Ag nanoparticles/PEDOT:PSS/PTB7:$PC_{71}BM$/Al (Fig. 4e). There are

Table 1 | Device characteristics of SY-based PLEDs and PTB7:$PC_{71}BM$-based PSCs with and without CD–Ag nanoparticles.

PLED configuration	Maximum luminance ($cd\ m^{-2}$) (at voltage)	Current efficiency ($cd\ A^{-1}$) (at voltage)	EQE (%) (at voltage)	Luminous efficiency ($lm\ W^{-1}$) (at voltage)
ITO/PEDOT:PSS/SY/LiF/Al	46,320 (11.6)	11.65 (7.4)	4.26 (7.4)	6.33 (4.8)
ITO/CD-Ag nanoparticles/PEDOT:PSS/SY/LiF/Al	46,460 (9.8)	27.16 (6.4)	9.07 (5.8)	18.54 (4.0)
PSC configuration	**J_{sc} ($mA\ cm^{-2}$)**	**V_{oc} (V)**	**FF**	**PCE (%)**
ITO/PEDOT:PSS/PTB7:$PC_{71}BM$/Al	14.4	0.75	0.70	7.53
ITO/CD-Ag nanoparticles/PEDOT:PSS/PTB7:$PC_{71}BM$/Al	16.0	0.75	0.70	8.31

negligible changes in the thickness and morphology of the active layer following the incorporation of CD–Ag nanoparticles (Supplementary Table S6). Figure 4f,g compares the current density versus voltage (J–V) characteristics and EQE of the devices with and without CD–Ag nanoparticles. The device without CD–Ag nanoparticles had a short-circuit current (J_{SC}) of 14.4 mA cm^{-2}, an open-circuit voltage (V_{OC}) of 0.75 V, a fill factor (FF) of 0.70 and a power conversion efficiency (PCE) of 7.53%. In contrast, the device with CD–Ag nanoparticles had a J_{SC} of 16.0 mA cm^{-2}, a V_{OC} of 0.75 V, a FF of 0.70 and a PCE of 8.31%. Detailed characteristics of the PSC devices are reported in Table 1. The inset of Fig. 4f shows the negligible effect of CD–Ag nanoparticles on dark J–V characteristics, which implies that the SPR effect by CD–Ag nanoparticles is more dominant than interfacial modification in device performance. This result is also supported by work function and conductivity measurements (Supplementary Fig. S7, Table S7). An improvement in the PCE of ~10% can be primarily attributed to the increase in J_{SC} caused by EQE enhancement in the range 400–700 nm, as shown in Fig. 4g, whereas the V_{OC} and FF remain similar. To clarify the effect of CD–Ag nanoparticles on the photogeneration of charge carriers, we compared the enhanced absorption ($\Delta\alpha$) and EQE (ΔEQE) of the CD–Ag nanoparticles (Fig. 4h). We measured reflectance spectra to evaluate absorption changes between devices with glass/CD–Ag nanoparticles/PEDOT:PSS/active layer/Al and glass/PEDOT:PSS/active layer/Al architectures (Supplementary Fig. S8)[37]. The EQE enhancement has two peaks at wavelengths of 430 nm and 630 nm, which are consistent with peaks in the $\Delta\alpha$ spectrum. We also compared the effect of free silver nanoparticles and CD–Ag nanoparticles on the device performance of PSCs using a mixture of poly(3-hexylthiophene) (P3HT) and [6,6]-phenyl-C_{61} butyric acid methyl ester (PCBM) (P3HT:PCBM) as the active layer (Supplementary Fig. S9, Table S8). Compared to the results for free silver nanoparticles, the devices with CD–Ag nanoparticles showed a higher PCE and broad EQE enhancement (Supplementary Fig. S9a,b). Because of the clustering effect of CD–Ag nanoparticles, the EQE enhancements by CD–Ag nanoparticles are efficient and broader than those of free silver nanoparticles, which are consistent with the corresponding UV–vis absorption spectrum (Supplementary Fig. S9c).

To determine the SPR effect of CD–Ag nanoparticles on internal quantum efficiency (IQE), we calculated the IQE by measuring the total absorption spectrum and EQE of the PTB7:$PC_{71}BM$-based PSCs (Fig. 5)[38,39]. The IQE is the ratio of the number of charge carriers collected by the solar cell to the number of photons of a given energy that shine on the solar cell from outside and are absorbed by the cell. It is surprising that the IQE value of PTB7:$PC_{71}BM$-based PSCs with CD–Ag nanoparticles is 99% at ~460 nm and that it stays near or even above 90% throughout the entire absorption spectrum (450–700 nm), whereas the IQE of the device without CD–Ag nanoparticles is below 91%. The CD–Ag nanoparticles lead to an IQE approaching 100%, which indicates that every absorbed photon results in a separated pair of charge carriers and that all photogenerated carriers are collected at the electrodes

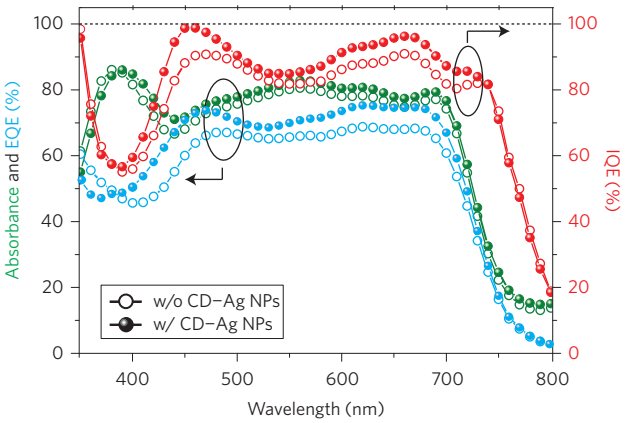

Figure 5 | IQE of PTB7:$PC_{71}BM$-based PSCs with CD–Ag nanoparticles. Red, blue and green lines show IQE, EQE and total absorption, respectively. Filled and open circles indicate device parameters with and without CD–Ag nanoparticles, respectively.

without any loss. To our knowledge, there is no report of an IQE enhancement approaching 100% following the introduction of plasmonic materials in PSCs. The PCE and IQE values of the device with CD–Ag nanoparticles are the highest reported to date for plasmonic PSCs using the SPR effect of metal nanoparticles (Supplementary Table S9).

In conclusion, we have demonstrated the synthesis of CD–Ag nanoparticles using carbon dots both as reducing agent and template, leading to broad light absorption originating from the ensemble plasmon coupling effect from clustering silver nanoparticles in CD–Ag nanoparticles. We also achieve a high current efficiency of 27.16 cd A^{-1} and a luminous efficiency of 18.54 lm W^{-1} in fluorescent PLEDs, as well as an IQE of 99% and a PCE of 8.31% in PSCs, using SPR enhancement with CD–Ag nanoparticles. These significant improvements in device efficiency demonstrate that SPR materials constitute a versatile and effective route to achieving high-performance PLEDs and PSCs. Furthermore, this approach shows promise as a route to the realization of electrically driven polymer lasers.

Methods

Fabrication and characterization of PLEDs and PSCs. A poly(*p*-phenylene vinylene) copolymer, Super Yellow (SY, Merck, $M_w = 1{,}950{,}000$ g mol^{-1}), was used for the PLED emission layer. A poly[[4,8-bis[(2-ethylhexyl)oxy]benzo[1,2-*b*:4,5-*b*′]dithiophene-2,6-diyl][3-fluoro-2-[(2-ethylhexyl)-carbonyl]thieno-[3,4-*b*]thiophenediyl]] (PTB7, 1-Material) and [6,6]-phenyl-C_{71} butyric acid methyl ester ($PC_{71}BM$, Rieke Metal) blend system was used for the active layer of the PSCs. Poly(3-hexylthiophene) (P3HT, Rieke Metal, $M_w = 50{,}000$ g mol^{-1}, ~95% regioregularity) and [6,6]-phenyl-C_{61} butyric acid methyl ester (PCBM, Rieke Metal) were used for the active layers in the solar cells. PEDOT:PSS (Baytron P VPAI 4083, H. C. Starck) was used for the hole-transporting layer in the PLEDs and PSCs. The device architecture used for the PLEDs and PSCs was ITO/CD–Ag nanoparticles/PEDOT:PSS/emission or active layer/(LiF)/Al. PLEDs and PSCs were fabricated using the following method. The CD–Ag nanoparticle composite solution was spin-cast at 2,000 r.p.m. on cleaned ITO substrates after UV–ozone

treatment for 10 min, and heated at 50 °C for 5 min in air. On top of the CD–Ag nanoparticle layer, PEDOT:PSS was spin-cast at 5,000 r.p.m. for 40 s and dried at 140 °C for 10 min. For the PLEDs, an SY solution (0.7 wt%) in chlorobenzene was spin-cast at 2,000 r.p.m., and LiF (0.5 nm) and Al (100 nm) electrodes were deposited on the emission layer under vacuum ($<1 \times 10^{-6}$ torr) by thermal evaporation. For the PSCs, a chlorobenzene solution consisting of PTB7 (1 wt%), $PC_{71}BM$ (1.5 wt%) and 1,8-diiodooctane (2 vol%) was spin-cast at 1,000 r.p.m. For solar cells incorporating P3HT:PCBM active layers, a mixture of P3HT (1 wt%) and PCBM (0.8 wt%) was spin-cast at 700 r.p.m. on top of the PEDOT:PSS layer in a nitrogen-filled glove box, and an aluminium electrode with a thickness of 100 nm was deposited on the active layer using the conditions as described for PLEDs. The area of the aluminium electrode defined the active area of the device as 13.5 mm^2. The electrical properties of the PLEDs were measured under ambient conditions using a Keithley 2400 source measurement unit equipped with a Minolta CS2000. The *J–V* characteristics of the PSCs were measured using a Keithley 2635A source measurement unit. Solar cell performance was tested with an AM1.5G solar simulator with an irradiation intensity of 100 mW cm^{-2}. EQE measurements were obtained using the PV measurement QE system by applying monochromatic light from a xenon lamp under ambient conditions. The monochromatic light intensity was calibrated using a silicon photodiode and chopped at 100 Hz. Masks (13.5 mm^2) made of thin metal were attached to each cell before measurement of the *J–V* characteristics and the EQE.

Received 22 January 2013; accepted 7 June 2013; published online 21 July 2013

References

1. Ren, J. *et al.* Blue (ZnSe) and green ($ZnSe_{0.9}Te_{0.1}$) light emitting diodes. *J. Cryst. Growth* **111,** 829–832 (1991).
2. AbuShama, J. A. M. *et al.* Properties of ZnO/CdS/$CuInSe_2$ solar cells with improved performance. *Progr. Photovolt. Res. Appl.* **12,** 39–45 (2004).
3. Britt, J. & Ferekides, C. Thin-film CdS/CdTe solar cell with 15.8% efficiency. *Appl. Phys. Lett.* **62,** 2851–2852 (1993).
4. Kim, J. Y. *et al.* Efficient tandem polymer solar cells fabricated by all-solution processing. *Science* **317,** 222–225 (2007).
5. He, Z. *et al.* Enhanced power-conversion efficiency in polymer solar cells using an inverted device structure. *Nature Photon.* **6,** 591–595 (2012).
6. Liang, Y. *et al.* For the bright future—bulk heterojunction polymer solar cells with power conversion efficiency of 7.4%. *Adv. Mater.* **22,** E135–E138 (2010).
7. Dou, L. *et al.* Tandem polymer solar cells featuring a spectrally matched low-bandgap polymer. *Nature Photon.* **6,** 180–185 (2012).
8. Small, C. E. *et al.* High-efficiency inverted dithienogermole-thienopyrrolodione-based polymer solar cells. *Nature Photon.* **6,** 115–120 (2012).
9. Choi, H. *et al.* Combination of titanium oxide and a conjugated polyelectrolyte for high-performance inverted-type organic optoelectronic devices. *Adv. Mater.* **23,** 2759–2763 (2011).
10. Kulkarni, A. P., Noone, K. M., Munechika, K., Guyer, S. R. & Ginger, D. S. Plasmon-enhanced charge carrier generation in organic photovoltaic films using silver nanoprisms. *Nano Lett.* **10,** 1501–1505 (2010).
11. Kumar, A., Srivastava, R., Tyagi, P., Mehta, D. S. & Kamalasanan, M. N. Efficiency enhancement of organic light emitting diode via surface energy transfer between exciton and surface plasmon. *Org. Electron.* **13,** 159–165 (2012).
12. Hutter, E. & Fendler, J. H. Exploitation of localized surface plasmon resonance. *Adv. Mater.* **16,** 1685–1706 (2004).
13. Atwater, H. A. & Polman, A. Plasmonics for improved photovoltaic devices. *Nature Mater.* **9,** 205–213 (2010).
14. Park, J. H. *et al.* Polymer/gold nanoparticle nanocomposite light-emitting diodes: enhancement of electroluminescence stability and quantum efficiency of blue-light-emitting polymers. *Chem. Mater.* **16,** 688–692 (2004).
15. Mathai, M. K., Choong, V-E., Choulis, S. A., Krummacher, B. & So, F. Highly efficient solution processed blue organic electrophosphorescence with 14 lm/W luminous efficacy. *Appl. Phys. Lett.* **88,** 243512 (2006).
16. Munechika, K. *et al.* Spectral control of plasmonic emission enhancement from quantum dots near single silver nanoprisms. *Nano Lett.* **10,** 2598–2603 (2010).
17. Heo, M. *et al.* High-performance organic optoelectronic devices enhanced by surface plasmon resonance. *Adv. Mater.* **23,** 5689–5693 (2011).
18. Baker, S. N. & Baker, G. A. Luminescent carbon nanodots: emergent nanolights. *Angew. Chem. Int. Ed.* **49,** 6726–6744 (2010).
19. Sun, Y-P. *et al.* Quantum-sized carbon dots for bright and colorful photoluminescence. *J. Am. Chem. Soc.* **128,** 7756–7757 (2006).
20. Zhu, H. *et al.* Microwave synthesis of fluorescent carbon nanoparticles with electrochemiluminescence properties. *Chem. Commun.* 5118–5120 (2009).
21. Lu, J. *et al.* One-pot synthesis of fluorescent carbon nanoribbons, nanoparticles, and graphene by the exfoliation of graphite in ionic liquids. *ACS Nano* **3,** 2367–2375 (2009).
22. Liu, H., Ye, T. & Mao, C. Fluorescent carbon nanoparticles derived from candle soot. *Angew. Chem. Int. Ed.* **46,** 6473–6475 (2007).
23. Liu, R. *et al.* An aqueous route to multicolor photoluminescent carbon dots using silica spheres as carriers. *Angew. Chem. Int. Ed.* **48,** 4598–4601 (2009).
24. Cao, L. *et al.* Carbon dots for multiphoton bioimaging. *J. Am. Chem. Soc.* **129,** 11318–11319 (2007).
25. Cao, L. *et al.* Carbon nanoparticles as visible-light photocatalysts for efficient CO_2 conversion and beyond. *J. Am. Chem. Soc.* **133,** 4754–4757 (2011).
26. Wang, F., Chen, Y-H., Liu, C-Y. & Ma, D-G. White light-emitting devices based on carbon dots' electroluminescence. *Chem. Commun.* **47,** 3502–3504 (2011).
27. Krysmann, M. J., Kelarakis, A., Dallas, P. & Giannelis, E. P. Formation mechanism of carbogenic nanoparticles with dual photoluminescence emission. *J. Am. Chem. Soc.* **134,** 747–750 (2011).
28. Neugart, F. *et al.* Dynamics of diamond nanoparticles in solution and cells. *Nano Lett.* **7,** 3588–3591 (2007).
29. Peng, J. *et al.* Graphene quantum dots derived from carbon fibers. *Nano Lett.* **12,** 844–849 (2012).
30. Selvi, B. R. *et al.* Intrinsically fluorescent carbon nanospheres as a nuclear targeting vector: delivery of membrane-impermeable molecule to modulate gene expression *in vivo*. *Nano Lett.* **8,** 3182–3188 (2008).
31. Wang, X. *et al.* Photoinduced electron transfers with carbon dots. *Chem. Commun.* 3774–3776 (2009).
32. Linic, S., Christopher, P. & Ingram, D. B. Plasmonic-metal nanostructures for efficient conversion of solar to chemical energy. *Nature Mater.* **10,** 911–921 (2011).
33. Kim, J-S., Friend, R. H., Grizzi, I. & Burroughes, J. H. Spin-cast thin semiconducting polymer interlayer for improving device efficiency of polymer light-emitting diodes. *Appl. Phys. Lett.* **87,** 023506 (2005).
34. Kim, H., Schulte, N., Zhou, G., Müllen, K. & Laquai, F. A high gain and high charge carrier mobility indenofluorene–phenanthrene copolymer for light amplification and organic lasing. *Adv. Mater.* **23,** 894–897 (2011).
35. Wang, D. *et al.* One- and two-photon absorption induced emission in HMASPS doped polymer. *Chem. Phys. Lett.* **354,** 423–427 (2002).
36. Namdas, E. B. *et al.* Low thresholds in polymer lasers on conductive substrates by distributed feedback nanoimprinting: progress toward electrically pumped plastic lasers. *Adv. Mater.* **21,** 799–802 (2009).
37. Kim, J. Y. *et al.* New architecture for high-efficiency polymer photovoltaic cells using solution-based titanium oxide as an optical spacer. *Adv. Mater.* **18,** 572–576 (2006).
38. Slooff, L. H. *et al.* Determining the internal quantum efficiency of highly efficient polymer solar cells through optical modeling. *Appl. Phys. Lett.* **90,** 143506 (2007).
39. Park, S. H. *et al.* Bulk heterojunction solar cells with internal quantum efficiency approaching 100%. *Nature Photon.* **3,** 297–302 (2009).

Acknowledgements

This research was supported by the WCU (World Class University) programme through the Korea Science and Engineering Foundation funded by the Ministry of Education, Science and Technology (R31-2008-000-20012-0), the National Research Foundation of Korea (grant 2009-0093020), the Korea Healthcare technology R&D Project, Ministry of Health & Welfare, Korea (A091047), and an International Cooperation of the Korea Institute of Energy Technology Evaluation and Planning (KETEP) grant funded by the Korea Government Ministry of Knowledge Economy (2012T100100740). The authors thank H-J. Shin for performing kelvin probe force microscopy for work function measurements.

Author contributions

H.C. designed and conducted most of the experiments, analysed the data and prepared the manuscript. S-J.K. performed PLEDs fabrication and characterization. T.K. and B.R.L. helped with the PLEDs fabrication experiments. Y.C. and P.J. contributed to the synthesis of carbon dots and characterization of CD–Ag nanoparticles by TEM, XPS and Raman spectroscopy. J-W.J. and J-R.J. performed FDTD calculations of the electric-field distribution of the CD–Ag nanoparticles. H.J.C. and M.C. contributed to ASE measurement. M.H.S. helped with interpreting data about PLEDs and ASE measurements. I-W.H. contributed to TCSPC measurements and data analysis. J.Y.K. and B-S.K. initiated the study, designed all the experiments, analysed the data and prepared the manuscript. All authors discussed the results and commented on the manuscript.

Additional information

Supplementary information is available in the online version of the paper. Reprints and permissions information is available online at www.nature.com/reprints. Correspondence and requests for materials should be addressed to B-S.K. and J.Y.K.

Competing financial interests

The authors declare no competing financial interests.